

Induction of sarcomas by mutant IDH2

Chao Lu,^{1,2} Sriram Veneti,¹ Altuna Akalin,^{3,4,11} Fang Fang,⁴ Patrick S. Ward,^{1,2} Raymond G. DeMatteo,¹ Andrew M. Intlekofer,¹ Chong Chen,¹ Jiangbin Ye,¹ Meera Hameed,⁵ Khedoudja Nafa,⁵ Narasimhan P. Agaram,⁵ Justin R. Cross,⁶ Raya Khanin,⁷ Christopher E. Mason,³ John H. Healey,⁸ Scott W. Lowe,^{1,9} Gary K. Schwartz,¹⁰ Ari Melnick,⁴ and Craig B. Thompson^{1,12}

¹Cancer Biology and Genetics Program, Memorial Sloan-Kettering Cancer Center, New York, New York 10065, USA; ²Cell and Molecular Biology Graduate Group, Perelman School of Medicine, University of Pennsylvania, Philadelphia, Pennsylvania 19104, USA; ³Department of Physiology and Biophysics, Institute for Computational Biomedicine, Weill Cornell Medical College, New York, New York 10065, USA; ⁴Division of Hematology/Oncology, Weill Cornell Medical College, New York, New York 10065, USA; ⁵Department of Pathology, Memorial Sloan-Kettering Cancer Center, New York, New York 10065, USA; ⁶Donald B. and Catherine C. Marron Cancer Metabolism Center, ⁷Bioinformatics Core, ⁸Orthopaedic Surgery Service, Memorial Sloan-Kettering Cancer Center, New York, New York 10065, USA; ⁹Howard Hughes Medical Institute, New York, New York 10065, USA; ¹⁰Melanoma and Sarcoma Service, Department of Medicine, Memorial Sloan-Kettering Cancer Center, New York, New York 10065, USA

More than 50% of patients with chondrosarcomas exhibit gain-of-function mutations in either isocitrate dehydrogenase 1 (IDH1) or IDH2. In this study, we performed genome-wide CpG methylation sequencing of chondrosarcoma biopsies and found that IDH mutations were associated with DNA hypermethylation at CpG islands but not other genomic regions. Regions of CpG island hypermethylation were enriched for genes implicated in stem cell maintenance/differentiation and lineage specification. In murine 10T1/2 mesenchymal progenitor cells, expression of mutant IDH2 led to DNA hypermethylation and an impairment in differentiation that could be reversed by treatment with DNA-hypomethylating agents. Introduction of mutant IDH2 also induced loss of contact inhibition and generated undifferentiated sarcomas in vivo. The oncogenic potential of mutant IDH2 correlated with the ability to produce 2-hydroxyglutarate. Together, these data demonstrate that neomorphic IDH2 mutations can be oncogenic in mesenchymal cells.

[*Keywords:* isocitrate dehydrogenase mutation; 2-hydroxyglutarate; differentiation; contact inhibition; tumorigenesis; DNA methylation; chondrosarcoma]

Supplemental material is available for this article.

Received July 16, 2013; revised version accepted August 16, 2013.

Nearly a century after Warburg (1956) observed that cancer cells metabolize glucose differently from quiescent tissues, the recent resurgence in cancer metabolism research has led to the increasing appreciation that metabolic reprogramming is a hallmark of cancer (Vander Heiden et al. 2009; Ward and Thompson 2012). However, it remains controversial whether metabolic reprogramming plays a significant role in the pathogenesis of cancer. An argument in support of this hypothesis is the identification of cancer-associated germline and somatic alterations of genes encoding for metabolic enzymes (Mullarky et al. 2011; Oermann et al. 2012), including the recent discovery of prevalent mutations in isocitrate dehydrogenase 1 (IDH1) and IDH2.

Cytosolic IDH1 and mitochondrial IDH2 are NADP⁺-dependent enzymes that metabolize isocitrate to α -ketoglutarate (α KG). Frequent somatic mutations of IDH1 and IDH2 were initially identified in ~80% of intermediate-grade gliomas (Yan et al. 2009) and ~20% of de novo acute myeloid leukemias (AMLs) (Mardis et al. 2009; Ward et al. 2010). More recently, they were also found in more than half of patients with chondrosarcomas (Amary et al. 2011a) and skeletal disorders characterized by cartilage tumors (Amary et al. 2011b; Pansuriya et al. 2011). Almost all mutations observed in IDH1 and IDH2 are monoallelic point mutations affecting only a few residues, suggesting that they are unlikely to be loss of function. Indeed, metabolomic and biochemical analysis revealed that mutant IDH enzymes gain a neomorphic activity of producing 2-hydroxyglutarate (2HG) from α KG (Dang et al. 2009; Ward et al. 2010). 2HG is normally present at very low levels in cells but exhibits a >100-fold increase in tumor samples with IDH mutations. It is believed that IDH mutations promote tumorigenesis through accumulating the putative "oncometabolite" 2HG.

¹¹Present address: Friedrich Miescher Institute for Biomedical Research, Maulbeerstrasse 66, 4058 Basel, Switzerland.

¹²Corresponding author
E-mail thompsonc@mskcc.org

Article is online at <http://www.genesdev.org/cgi/doi/10.1101/gad.226753.113>.

At the molecular level, mounting evidence implicates a link between IDH mutation and epigenetic dysregulation. In hematologic tumors and gliomas, IDH mutations are associated with a DNA hypermethylation profile and a gene expression pattern associated with lineage-specific progenitors (Figuroa et al. 2010; Noushmehr et al. 2010; Turcan et al. 2012). Mechanistically, mutant IDH was shown to impair activities of α KG-dependent chromatin-modifying enzymes by producing 2HG as a competitive inhibitor. These include TET family enzymes, which convert 5-methylcytosine (5mC) to 5-hydroxymethylcytosine (5hmC), a novel epigenetic mark potentially involved in DNA demethylation (Figuroa et al. 2010). Similarly, 2HG-producing IDH mutation inhibits activities of α KG-dependent Jumonji-C histone demethylases and leads to increased methylation at certain histone lysine residues (Chowdhury et al. 2011; Xu et al. 2011; Lu et al. 2012).

Although the high frequencies of IDH mutations in cancer imply that they are potential “driver” mutations, *in vitro* and *in vivo* modeling of IDH mutations has yet to report overt cellular transformation. Introduction of a mutant *IDH1* allele as either a transgene or knock-in into hematopoietic cells, neural progenitors, or immortalized cell lines has failed to produce tumors *in vivo* (Sasaki et al. 2012b; Turcan et al. 2012). To date, the properties of IDH mutant tumors of mesenchymal origin have not been characterized, and the role of IDH mutations in the tumorigenesis of such cells has not been examined. As in other tumor types, we now report that IDH mutation is associated with extensive changes in DNA methylation that are enriched at promoter CpG islands of genes implicated in the regulation of cellular differentiation. Similar changes were observed when an *IDH2* mutant allele was introduced into immortalized mesenchymal cells. Furthermore, in such cells, expression of mutant IDH2 leads to impaired mesenchymal lineage differentiation and loss of contact inhibition *in vitro* and formation of mesenchymal tumors *in vivo*. Abolishing 2HG-producing activity from mutant IDH2 eliminates its transformation capacity. Collectively, the data presented here demonstrate that the 2HG-producing IDH2 mutation can directly induce tumor formation *in vivo*.

Results

Genome-wide DNA methylation landscape of IDH mutant chondrosarcomas

A panel of snap-frozen surgical specimens from 21 patients with chondrosarcomas was collected through an institutional review board-approved protocol. Targeted sequencing results revealed an ~50% frequency of IDH mutations in chondrosarcomas (seven of the samples had the R132 *IDH1* mutation, three had the R172 *IDH2* mutation, and 11 were wild type for *IDH1/2*), consistent with previous reports (Amary et al. 2011a; Pansuriya et al. 2011; Arai et al. 2012). Compared with samples that were wild type for *IDH1/2*, *IDH1* or *IDH2* mutant samples

showed a significant increase in intratumoral 2HG levels (Fig. 1A).

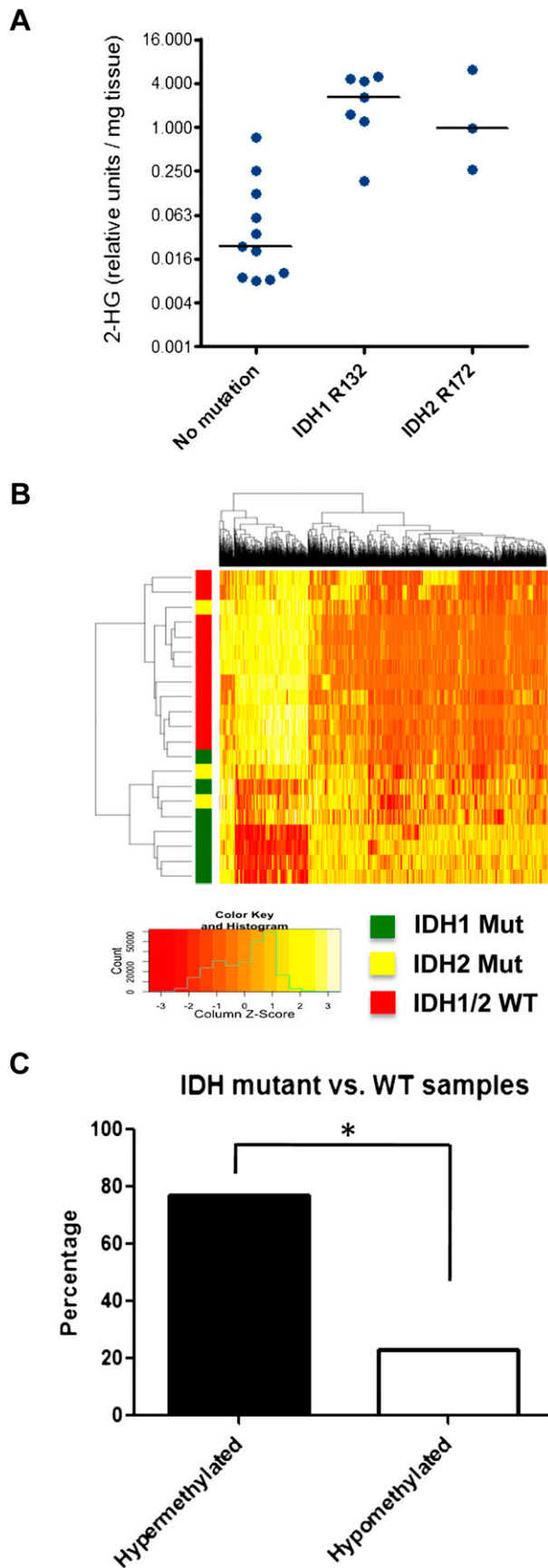
Genome-wide DNA methylation levels were measured using enhanced reduced representation bisulfite sequencing (ERRBS), which was previously demonstrated to provide base-pair resolution DNA methylation information and extended genomic coverage beyond CpG island regions compared with traditional RRBS (Akalin et al. 2012a). A minimum cutoff of 40% methylation difference, in addition to statistical significance ($Q < 0.01$), was required to identify differentially methylated CpGs between *IDH1/2* wild-type and mutant samples. A total of 12,236 CpGs were found to be differentially methylated.

Individual CpG sites were next annotated to CpG islands, shores, or regions beyond CpG shores. The results showed that *IDH1/2* mutations were associated with DNA hypermethylation at CpG islands (77% of differentially methylated CpGs were hypermethylated in *IDH1/2* mutant samples) (Fig. 1B,C). In contrast, a minority of CpG shores and other regions (29% and 3%, respectively) displayed increased methylation in IDH mutant samples.

Analysis of DNA methylation at gene promoters was performed by selecting differentially methylated CpGs at -1000 to $+500$ base pairs (bp) of each transcription start site. The group of genes that were promoter DNA-hypermethylated in IDH mutant chondrosarcomas was then subjected to Database for Annotation, Visualization, and Integrated Discovery (DAVID) analysis to examine their functional relevance. The results showed that the top enriched functional categories were involved in various organismal and cellular developmental processes (Supplemental Fig. S1; Supplemental Table S1). In addition, the most significantly hypermethylated genes in IDH mutant samples include lineage specification regulators such as retinoic acid receptor α (*RARA*), platelet-derived growth factor receptor α (*PDGFRA*), and BCL6 corepressor (*BCOR*) (Supplemental Table S2). Taken together, these data provide a comprehensive genome-wide DNA methylation landscape of IDH mutant chondrosarcomas and suggest that IDH mutations are associated with epigenetic dysregulation of genes implicated in the regulation of stem cell maintenance/differentiation and cell lineage specification.

IDH2 mutation induces DNA hypermethylation

To establish the causality between IDH mutation and aberrant DNA methylation, the DNA methylome between isogenic cell lines expressing wild-type or mutant IDH was compared. In contrast to others, we chose to examine the role of chondrosarcoma-associated mitochondrial IDH2 mutants. Unlike cytosolic IDH1 R132 mutants, mitochondrial IDH2 R172 mutants generate high levels of their neomorphic product, 2HG, independently of the action of wild-type enzymes (Ward et al. 2013). We retrovirally transduced 10T1/2 (10T) cells with vectors containing either wild-type or R172K mutant IDH2. 10T cells expressing R172K mutant IDH2 but not empty vector or wild-type IDH2 showed significant accumulation of 2HG (Supplemental Fig. S2).



Genomic DNA of 10T cells was extracted and processed for ERRBS to generate highly reproducible base-pair resolution DNA methylation profiles (Supplemental Fig. S3A). In agreement with results from chondrosarcoma biopsies, IDH2 R172K mutant cells compared with wild-type cells showed a profound DNA hypermethylation at CpG islands across all chromosomes (Fig. 2A). In contrast, significantly less differentially methylated CpGs were observed between wild-type IDH2 and vector cells, with even distribution of hypermethylated and hypomethylated sites (Fig. 2A). Increased methylation at several histone marks, such as H3K9me3, H3K9me2, and H3K4me3, was also found in IDH2 R172K mutant cells, which could reinforce with DNA methylation to modulate gene expression (Supplemental Fig. S3B).

In total, there were 2400 genes with differentially methylated CpGs at their promoters, and a predominance in DNA hypermethylation was observed when comparing the IDH2 R172K mutant with wild-type cells (78.1% being hypermethylated, P -value < 0.0001) (Supplemental Table S3). To gain more insights into the mechanism of aberrant DNA methylation, the group of genes that were promoter DNA-hypermethylated in IDH2 R172K mutant cells was subjected to gene set enrichment analysis (GSEA) with the Broad Institute Molecular Signatures Database (<http://www.broadinstitute.org/gsea/msigdb/index.jsp>), which includes >3000 curated gene sets collected from various research sources. The top four most statistically significantly enriched gene sets were Polycomb-repressive complex 2 (PRC2) target genes or genes marked by H3K27me3 in embryonic stem cells (Fig. 2B; Supplemental Table S4). Notably, recent genome-wide mapping of Tet1-binding sites revealed that >95% of PRC2 target genes were bound by Tet1 (Wu and Zhang 2011), and Tet1 has been proposed as a guardian to protect these regions from accidental DNA methylation (Williams et al. 2012). Taken together, the DNA methylome analysis suggests that acquisition of an IDH2 R172 mutation is sufficient to establish DNA hypermethylation, the pattern of which matches the patterns of Tet1- and PRC2-binding activity.

Figure 1. ERRBS analysis of chondrosarcoma patient samples. (A) Twenty-one blinded chondrosarcoma samples were analyzed for 2HG levels by gas chromatography-mass spectrometry (GC-MS). Subsequently, samples were decoded and grouped according to IDH1/2 mutational status. (B) ERRBS was performed on genomic DNA extracted from chondrosarcoma patient samples to generate genome-wide base-pair resolution CpG methylation information. A heat map representing the hierarchical clustering of samples with wild-type (WT) or mutant IDH1/2 is shown, based on a supervised analysis for differentially methylated CpGs at CpG islands. Each row represents a sample, and each column represents a CpG. The level of methylation is represented using a color scale, as shown in the legend. (C) Bar graph showing the percentage of hypermethylated and hypomethylated CpGs comparing IDH1/2 mutant with wild-type chondrosarcoma samples. (*) $P < 0.0001$ by χ^2 test.

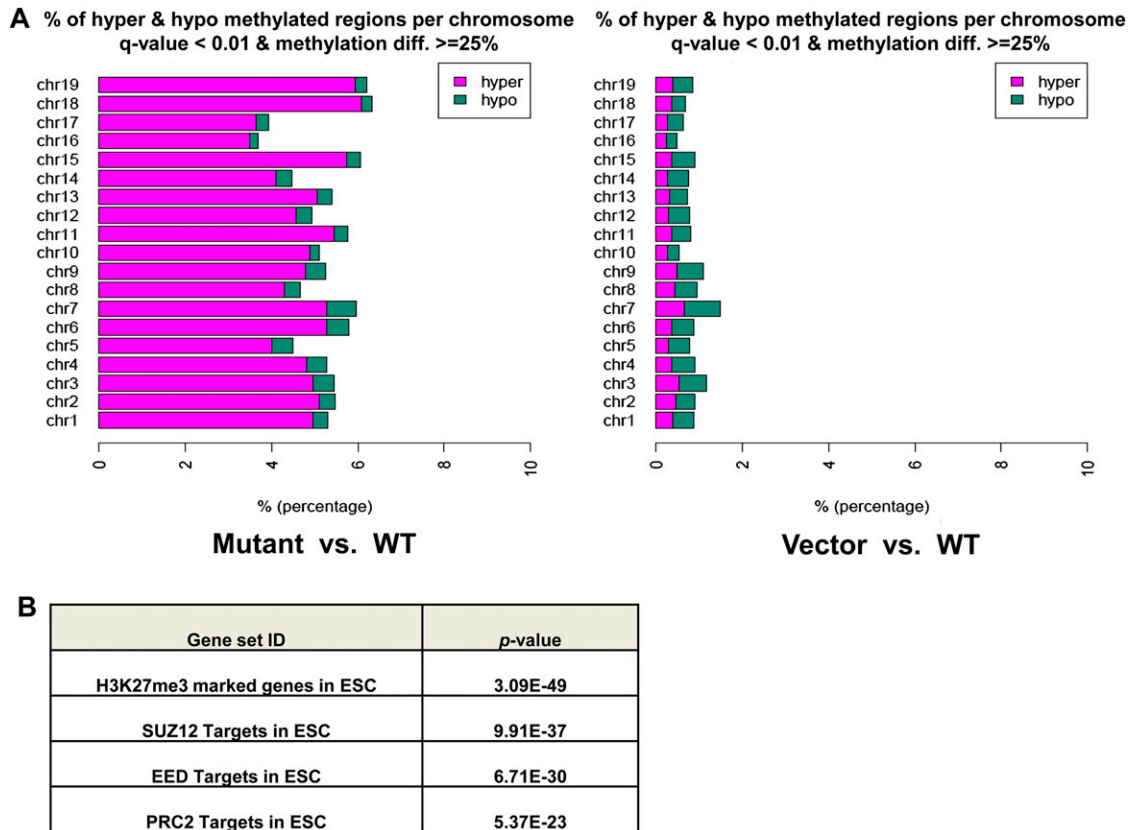


Figure 2. Mutant IDH2 induces CpG island hypermethylation phenotype. (A) Stacking bar graph showing percentage of hypermethylated and hypomethylated CpGs of all CpGs located in CpG islands for each chromosome, comparing IDH2 R172K mutant with wild-type (WT) cells (*left*) or vector with IDH2 wild-type cells (*right*). Green represents proportion of hypomethylated cytosines, and magenta represents hypermethylated ones. Only CpGs with a Q-value < 0.01 and a methylation difference of at least 25% are shown. (B) GSEA was performed on genes that were promoter DNA-hypermethylated in IDH2 R172K mutant cells. The table shows the top four most significantly enriched gene sets from the Broad Institute database and their P-values.

Mutant IDH2 inhibits mesenchymal lineage differentiation

10T cells were originally isolated from C3H mouse embryos. They were demonstrated to be multipotent, with the ability to differentiate into several mesenchymal lineages, including adipocytes, myoblasts, and chondrocytes (Taylor and Jones 1979). Since the DNA methylation signature associated with IDH mutant chondrosarcomas was enriched for stem cell maintenance and differentiation genes, the effects of IDH2 mutation on the mesenchymal differentiation potential of 10T cells were determined. Expression of R172K mutant IDH2 in 10T cells led to a profound impairment in either adipocyte or chondrocyte differentiation. Compared with vector and wild-type IDH2 cells, IDH2 R172K mutant cells showed no visible accumulation of lipid droplets and failed to express mature adipocyte markers (*Adipoq* and *Fabp4*) after adipocyte differentiation induction (Fig. 3A). Similarly, when cells were subjected to conditions that promote chondrocyte differentiation, morphological conversion to rounded shapes resembling mature chondrocytes and expression of mature chondrocyte markers (*Acan* and *Col2a1*) were only observed in vector and wild-type IDH2 cells, while IDH2 R172K mutant cells

maintained a fibroblast-like undifferentiated state (Fig. 3B). Notably, overexpression of wild-type IDH2 enzyme led to enhanced expression of mature chondrocyte markers, suggesting that increased production of NADPH and α KG may promote cellular differentiation. Furthermore, while vector and wild-type IDH2 cells became proliferation-arrested after the induction of adipocyte or chondrocyte differentiation, the proliferation rate of IDH2 R172K mutant cells remained largely unaffected (Fig. 3C). IDH2 R172K mutant cells were also able to maintain cyclin D1 levels after differentiation induction, unlike vector and wild-type IDH2 cells (Fig. 3D).

Differentiation impairment by mutant IDH2 correlates with high levels of 2HG accumulation

We previously demonstrated that a rare mutation in IDH1 (A134D) identified in thyroid cancers abolished the catalytic activity of the enzyme (Ward et al. 2012). To determine whether the 2HG-producing activity is required for R172K mutant IDH2 to inhibit differentiation, a similar mutation was introduced to the analogous residue in IDH2 (A174D), which is predicted to interfere with the substrate binding of R172 and eliminate the enzymatic activity of R172K mutant IDH2 (Fig. 4A).

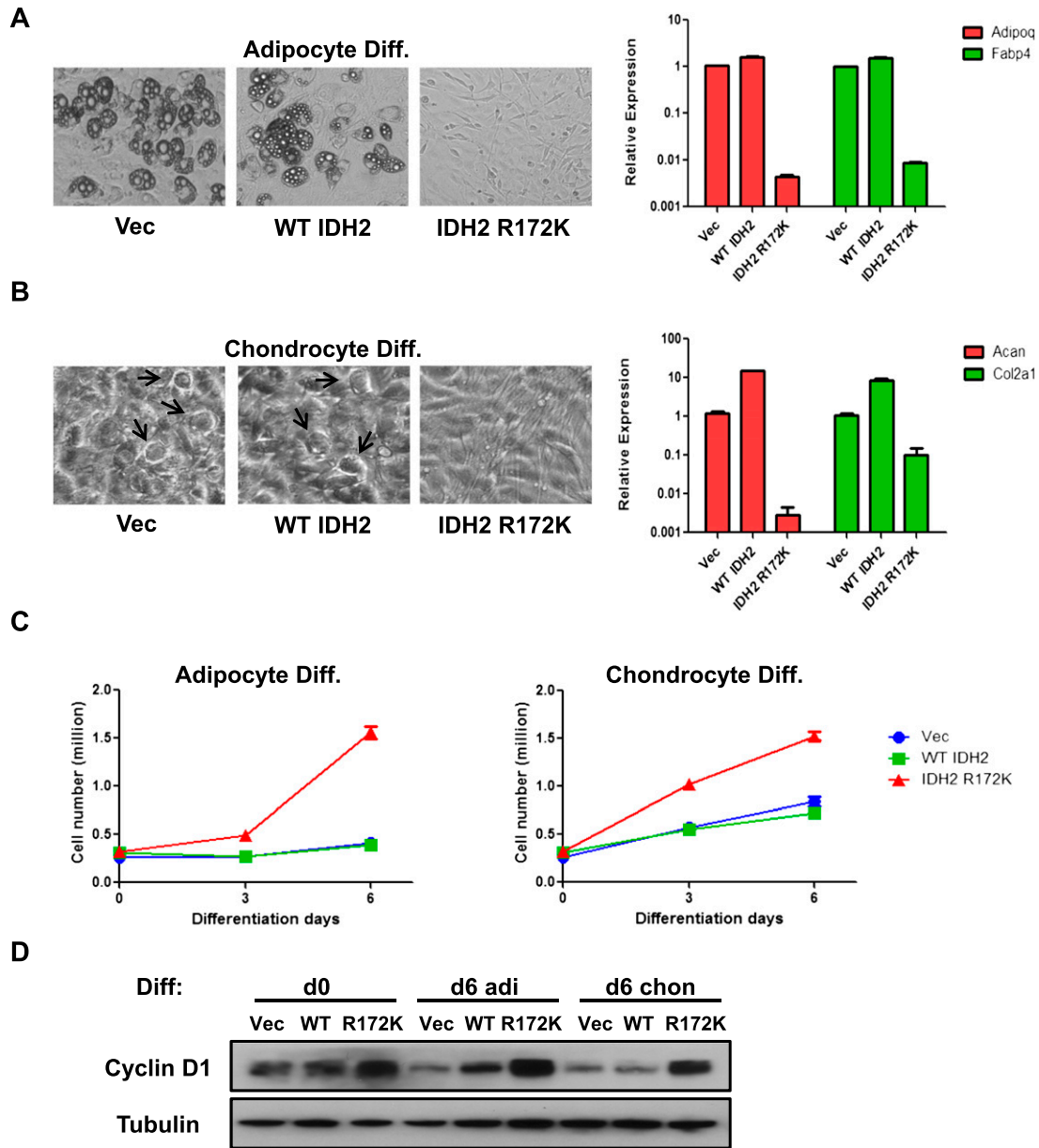


Figure 3. IDH2 mutation inhibits mesenchymal differentiation. (A) Vector (Vec), wild-type (WT), or R172K mutant IDH2 cells were treated with adipocyte differentiation cocktail. After 7 d of differentiation induction, representative microscopic images of cell morphology were recorded, and mRNA expression of *Adipoq* and *Fabp4* was measured by quantitative real-time PCR (qRT-PCR). (B) Vector, wild-type, or R172K mutant IDH2 cells were treated with chondrocyte differentiation cocktail. After 10 d of differentiation induction, representative microscopic images of cell morphology were recorded (arrowheads point to mature chondrocyte-resembling cells), and mRNA expression of *Acan* and *Col2a1* was measured by qRT-PCR. (C) 10T vector, wild-type, or R172K mutant IDH2 cells were treated with adipocyte or chondrocyte differentiation cocktails. Cell numbers were counted at days 0, 3, and 6 after differentiation induction. (D) Six days after adipocyte or chondrocyte differentiation induction, 10T vector, wild-type, or R172K mutant IDH2 cells were lysed, and protein levels of cyclin D1 were measured by Western blot. Tubulin was used as loading control. For all experiments, the average \pm SD from three biological replicates are shown.

Indeed, 2HG levels in 10T cells stably expressing R172K/A174D mutant IDH2 were comparable with vector and wild-type IDH2 cells (Fig. 4B). 10T cells stably expressing R140Q mutant IDH2 were also generated. R140Q mutation in IDH2 is only found in hematological malignancies and was shown to be a weak 2HG-producing mutant (Ward

et al. 2013). In 10T cells, expression of R140Q mutant IDH2 increased 2HG levels by fivefold, while R172K mutant IDH2 increased 2HG levels by >100-fold (Fig. 4B). When cells were tested for their differentiation potentials, the A174D mutation was found to abolish R172K mutant IDH2's ability to block adipocyte or chondrocyte

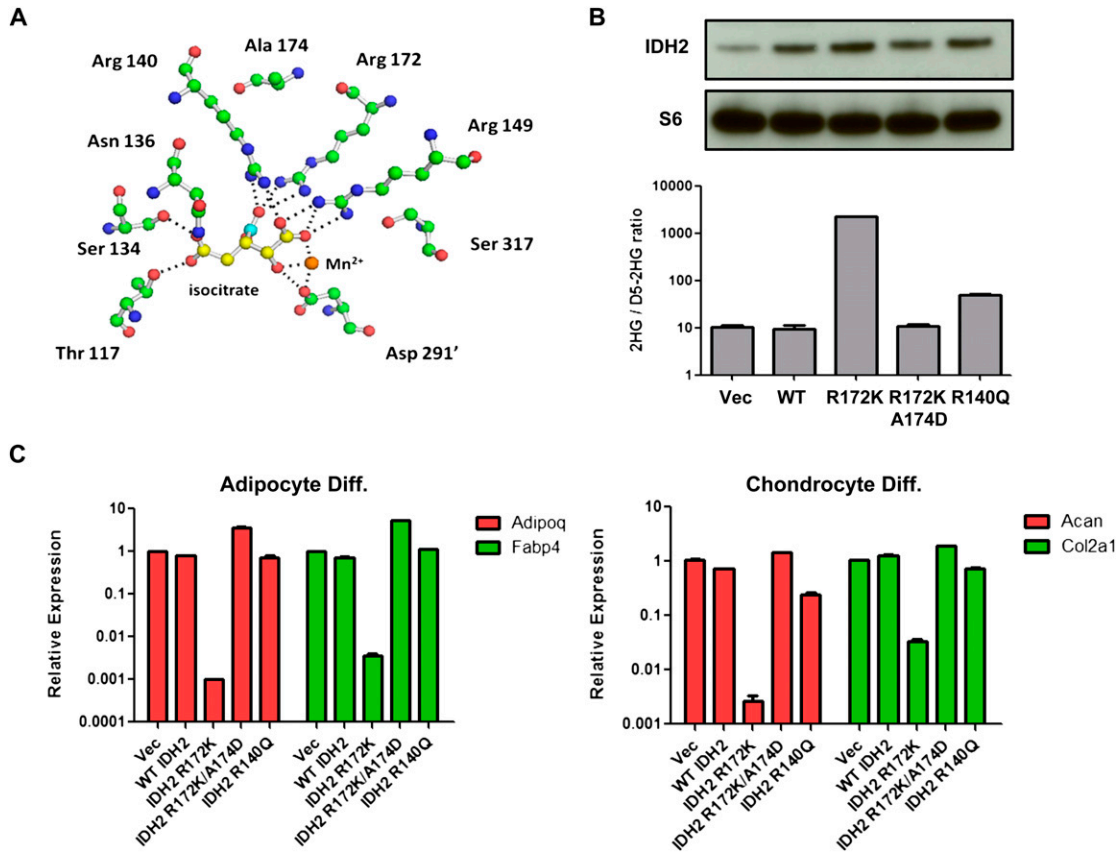


Figure 4. Differentiation impairment by mutant IDH2 correlates with 2HG production. (A) Structural modeling of IDH2 catalytic site showing Arg 172 and Ala 174. Isocitrate carbons are in yellow except carbon 6 containing the β -carboxyl, which is highlighted in cyan. Carbon atoms of amino acids (green), amines (blue), and oxygens (red) are also depicted. Hydrogen atoms are omitted for clarity. Dashed lines show <3.1 Å interactions corresponding to hydrogen and ionic bonds. The prime (') denotes that the residue comes from the other monomer of the IDH dimer. (B) 10T cells expressing vector (Vec), wild-type (WT), R172K, R172K/A174D, or R140Q mutant IDH2 were lysed, and IDH2 expression was measured by Western blot. 2HG levels were measured by GC-MS and normalized to internal standard (D5-2HG) and cell number. (C) 10T cells expressing wild-type or various mutant IDH2 were treated with adipocyte or chondrocyte differentiation cocktails. mRNA expression of *Adipoq*, *Fabp4*, *Acan*, and *Col2a1* was measured by qRT-PCR after 8 d of differentiation induction. For all experiments, the average \pm SD from three biological replicates are shown.

differentiation (Fig. 4C). Similarly, weak 2HG-producing R140Q mutant IDH2 did not result in any differentiation impairment.

DNA-hypomethylating treatment reverses differentiation block by mutant IDH2

To functionally link DNA hypermethylation to differentiation impairment, IDH2 R172K mutant cells were treated with 5-azacytidine (5-aza) to test whether inhibiting DNA methyltransferase had any effect on reversing the differentiation inhibition by mutant IDH2. After treatment with low doses of 5-aza for 48 h to induce global DNA demethylation (Supplemental Fig. S4), IDH2 R172K mutant cells were allowed to proliferate in the absence of 5-aza until reaching confluence before being subjected to adipocyte differentiation induction. Compared with untreated cells, a transient exposure to 5-aza led to the accumulation of lipid droplets and a dose-dependent increase in the expression of mature adipocyte

markers (*fabp4* and *adipoq*) after 8 d of differentiation induction (Fig. 5A,B), suggesting that IDH2 R172K mutant cells' differentiation potential can be restored upon treatment with a DNA-hypomethylating agent.

IDH2 mutant cells escape contact inhibition

In addition to mesenchymal multipotency, 10T cells are sensitive to confluence-induced proliferation arrest and show no tumorigenicity in xenograft studies (Reznikoff et al. 1973). However, the differentiation experiments described above require cells to be seeded at confluence before induction. Therefore, the findings that IDH2 R172K mutant cells were able to continue proliferation at post-confluence (Fig. 3C,D) prompted us to investigate whether these cells, in addition to differentiation impairment, have acquired resistance to contact inhibition. When cultured in normal growth medium, vector, wild-type IDH2, or IDH2 R172K mutant cells showed no difference in proliferation rate when cells were sparse

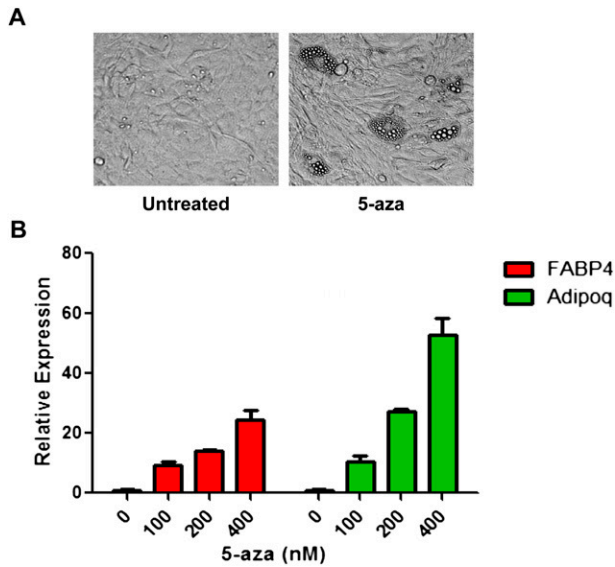


Figure 5. DNA-hypomethylating agent reverses the differentiation defect in mutant IDH2 cells. (A) After 8 d of adipocyte differentiation induction, microscopic images of cell morphology were recorded in IDH2 R172K mutant cells with or without transient 5-aza treatment. (B) After 8 d of adipocyte differentiation induction, mRNA expression of *Adipoq* and *Fabp4* in IDH2 R172K mutant cells with or without transient 5-aza treatment was measured by qRT-PCR. The average \pm SD from three biological replicates are shown.

(days 0–2) (Fig. 6A). However, while vector and wild-type IDH2 cells stopped proliferating shortly after reaching confluence (days 2–6), the accumulation of IDH2 R172K mutant cells continued even after confluence was achieved. Measurement of cell mitotic activity by detection of the incorporation of nucleoside analog 5-ethynyl-2'-deoxyuridine (EdU) also revealed that IDH2 R172K mutant cells were more mitotically active at post-confluence (Fig. 6B). Moreover, compared with vector and wild-type IDH2 cells, the induction of the cell cycle inhibitor p27 and the decrease in cyclin D1 levels after contact inhibition were less pronounced in IDH2 R172K mutant cells (Fig. 6C). These features were not observed in IDH2 R172K/A174D or R140Q mutant cells (Fig. 6D), suggesting that loss of contact inhibition induced by mutant IDH2 requires high levels of 2HG production.

IDH2 R172K mutant cells underwent cell cycle arrest normally after serum deprivation (Supplemental Fig. S5A), suggesting that their escape from contact inhibition is unlikely to be due to defects in cell cycle regulation. The cadherins are critical components of cell–cell adhesion and have been proposed as the main upstream mediator of contact inhibition (Gumbiner 2005). Unlike vector and wild-type IDH2 cells, IDH2 R172K mutant cells failed to up-regulate N-cadherin protein and mRNA expression after reaching confluence (Fig. 6E), suggesting that the post-confluence growth of these cells results from the inability to sense cell–cell contact at the surface membrane. This may be at least in part due to epigenetic gene silencing, as two cell adhesion genes (*Itga9* and *ctnn1*) that

were DNA-hypermethylated in IDH2 R172K mutant cells (Supplemental Table S3) failed to increase their mRNA expression upon cell–cell contact (Supplemental Fig. S5B).

IDH2 mutant cells generate poorly differentiated sarcomas in vivo

Given the malignant phenotypes of differentiation blockade and loss of contact inhibition observed in vitro, xenograft studies were performed to test whether 10T cells with IDH2 mutation could generate tumors in vivo. IDH2 R172K mutant cells formed palpable tumors 20 d after subcutaneous injection and continued to grow up to 1000 mm³, while vector and wild-type IDH2 cells showed no tumorigenicity over the course of study (Fig. 7A). Immunohistochemistry staining revealed that these tumors resembled poorly differentiated sarcomas with a high Ki67 index (Fig. 7B). Consistent with in vitro studies, these tumors also had high levels of cyclin D1, low p27 expression (Fig. 7B), and no detectable staining for mature mesenchymal lineage markers (data not shown). Tumors from IDH2 R172K mutant cells showed 2HG levels that were comparable with cells cultured in vitro (Fig. 7C), and IDH2 R172K/A174D or R140Q mutant cells failed to induce xenograft growth (Fig. 7D).

Discussion

The study of IDH mutations in carcinogenesis has been hampered by a lack of robust model systems. We previously found that IDH mutation blocked adipocyte differentiation from 3T3-L1 murine fibroblasts (Lu et al. 2012). This finding has been extended to the hematopoietic system with the observations that mutant IDH and 2HG could impair EPO-induced erythrocyte differentiation in an erythroleukemic cell line (Losman et al. 2013) and that hematopoietic conditional knock-in IDH1 mutant mice had an expansion in early progenitor/stem cell population (Sasaki et al. 2012b). Nevertheless, none of the previous studies reported in vivo tumorigenicity as a result of the presence of mutant IDH. We report here that, using a nontransformed mesenchymal multipotent cell line, expression of an IDH2 mutant enzyme producing high levels of 2HG not only arrested cells from differentiating into adipocytic and chondrocytic lineages, but also resulted in loss of contact inhibition and tumor formation in vivo. It is noteworthy that 10T cells have been frequently used as an in vitro model to test the carcinogenic potential of chemicals in mesenchymal cells (for review, see Schechtman 2012). While it is possible that pre-existing genetic and epigenetic alterations in 10T cells render them more susceptible to 2HG-induced transformation, the in vivo tumorigenicity established here depends on the introduction of a 2HG-producing IDH2 R172K mutant transgene. The morphology of the mutant IDH2-induced 10T tumors in vivo resembles that of human chondrosarcomas in which the block to cartilage formation becomes more pronounced as the tumor progresses. This is consistent with the in vitro impairment in cell differentiation exhibited by 10T cells

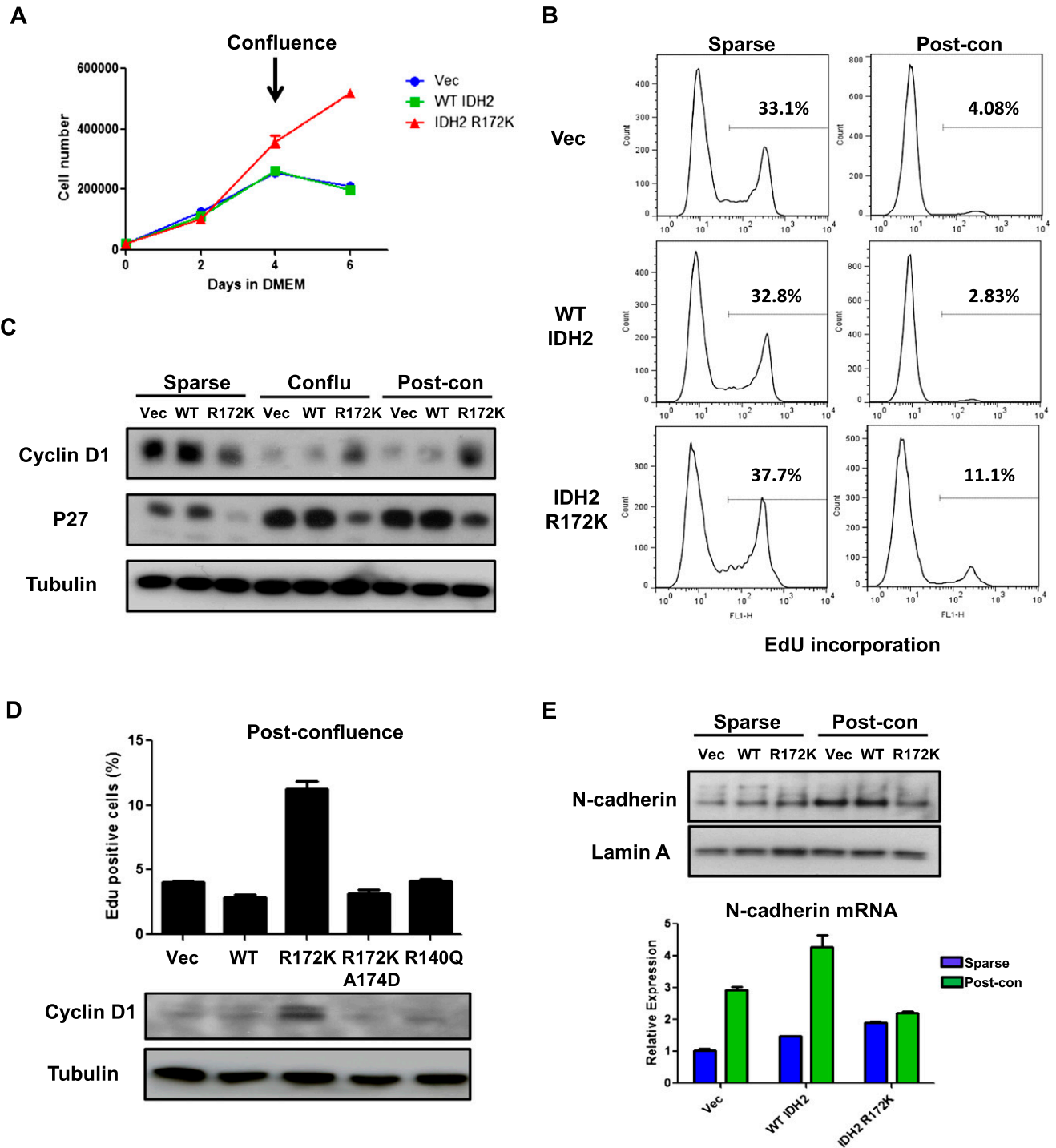


Figure 6. IDH2 mutant cells show loss of contact inhibition. (A) 10T vector (Vec), wild-type (WT), or R172K mutant IDH2 cells were cultured in Dulbecco's modified Eagle's medium (DMEM), and cell numbers were counted at days 0, 2, 4, and 6. Cells reached confluence between days 2 and 4. (B) Vector, wild-type, or R172K mutant IDH2 cells at sparse or post-confluence day 2 were incubated with EdU for 4 h. Percentage of EdU-positive cells was measured by flow cytometry. Histograms from a representative experiment from a total of two experiments are shown. (C) Vector, wild-type, or R172K mutant IDH2 cells were lysed at sparse, confluence, or 2 d post-confluence. Protein levels of cyclin D1 and p27 were measured by Western blot. Tubulin was used as loading control. (D) 10T cells expressing wild-type or various mutant IDH2s at post-confluence day 2 were incubated with EdU for 4 h. Percentage of EdU-positive cells was measured using flow cytometry. Cells were also lysed, and cyclin D1 levels were measured by Western blot. Tubulin was used as loading control. (E) Vector, wild-type, or R172K mutant IDH2 cells were lysed at sparse or 2 d post-confluence. Levels of N-cadherin protein expression were measured by Western blot, and mRNA expression was measured by qRT-PCR. For all experiments, the average \pm SD from three biological replicates are shown.

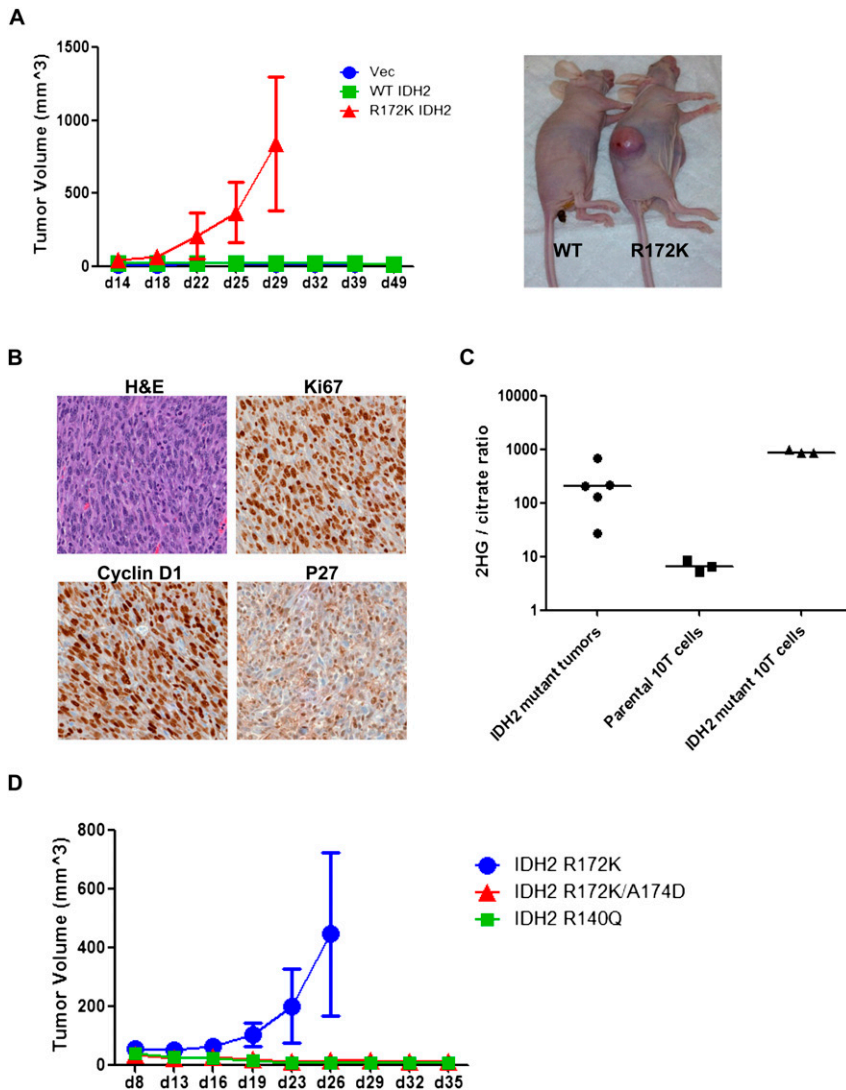


Figure 7. IDH2 mutant cells generate mesenchymal tumors in vivo. (A) We injected 1×10^7 10T vector (Vec), wild-type (WT), or R172K mutant IDH2 cells subcutaneously into nude mice. Tumor growth was monitored and measured. The *insert* image is shown for mice implanted with wild-type cells (*left*) or mutant cells (*right*) at the time of sacrifice. (B) Immunohistochemical staining was performed on R172K mutant IDH2 tumors using specific antibodies, and representative images are shown for sections stained with hematoxylin and eosin (H&E), Ki67, cyclin D1, and p27. (C) 2HG levels in R172K mutant IDH2 tumors and parental or R172K mutant IDH2 10T cells cultured in vitro were measured by GC-MS. The ratio of 2HG to citrate is shown. (D) We injected 1×10^7 10T R172K, R172K/A174D, or R140Q mutant IDH2 cells subcutaneously into nude mice. Tumor growth was monitored and measured. For all experiments, the average tumor volumes \pm SD of five mice per group are shown.

expressing a chondrosarcoma-associated IDH2 R172K mutant enzyme.

As a common product of recurrent cancer-associated IDH1 and IDH2 mutations, 2HG is believed to mediate mutant IDH's tumor-promoting potential. We and others have shown that exogenous 2HG could recapitulate mutant IDH's effect on blocking cell differentiation (Lu et al. 2012; Losman et al. 2013). In the present study, we further demonstrate that high levels of 2HG production were required for mutant IDH2's transformation capacity. Therefore, it appears that enzymatic activity is necessary for oncogenesis by mutant IDH. It should be noted that the truncated reverse reaction catalyzed by mutant IDH also consumes NADPH. Since the R172K/A174D mutant IDH2 was enzymatically inactive, our experiments do not rule out the possibility that NADPH consumption and the resulting generation of reactive oxygen species (ROS) are also important for mutant IDH's oncogenic mechanism. However, since IDH mutations in cancer are monoallelic and the reverse reaction by mutant IDH occurs at a much slower rate compared with the

forward reaction by the wild-type enzyme (Dang et al. 2009), the mutation's impact on the total cellular NADPH pool is likely to be minimal. In agreement, studies have shown that the intracellular ROS levels actually decrease as a result of mutant IDH expression (Sasaki et al. 2012a; Li et al. 2013).

In agreement with previous findings in other tumor types, quantitative profiling of genome-wide DNA methylation using ERRBS revealed a significant increase in CpG island methylation in IDH mutant chondrosarcoma samples. Such association is unlikely to result from the disparate cells of origin affected by IDH mutations, as the expression of the IDH2 R172K mutant in 10T cells was sufficient to cause CpG island DNA hypermethylation. GSEA showed a remarkable overlap between R172K mutant IDH2-associated promoter-hypermethylated genes and PRC2 target/Tet1-bound genes in embryonic stem cells. Since other cell types, including mesenchymal progenitor cells, show a similar PRC2 target preference (Bracken et al. 2006; Squazzo et al. 2006), our results suggest that the establishment of DNA hypermethylation by mutant

IDH2 in 10T cells may be the result of TET inhibition. Importantly, functional analysis and validation experiments implicate that aberrant promoter DNA methylation may underlie the inability to regulate the expression of genes important for differentiation and cell–cell contact. Consistent with this notion, we showed that low-dose pulsing of 5-aza, which has been shown to exert durable anti-tumor activities (Tsai et al. 2012), was sufficient to reverse the differentiation defect of IDH2 mutant cells. Therefore, IDH mutation may initiate and promote tumorigenesis by epigenetically “locking” a proliferative progenitor cell in that state.

Recently, inhibitors that specifically abrogate mutant IDH's ability to produce 2HG have been developed (Wang et al. 2013). It was shown that the inhibitors could induce differentiation, delay xenograft growth, and reverse histone hypermethylation in tumor cells containing ectopic or endogenous mutant IDH (Rohle et al. 2013; Wang et al. 2013), suggesting that some of the epigenetic abnormalities are potentially correctable. To date, no inhibitors of 2HG production by the chondrosarcoma-associated IDH2 R172 mutation studied here have been reported. However, given 2HG's remarkable impact on the epigenome, it would be interesting to test whether compounds targeting chromatin modifiers are selectively toxic to tumors with an IDH mutation.

Materials and methods

Chondrosarcoma patient samples and ERRBS analysis

Acquisition of snap-frozen surgical tumor specimens from patients with chondrosarcomas was carried out through a Memorial Sloan-Kettering Cancer Center institutional review board-approved protocol. MALDI-TOF mass spectrometry (MS) (Sequenom) platform was used to identify IDH1/2 mutations. ERRBS was performed with genomic DNA extracted from 10T cells or chondrosarcoma biopsies as previously described (Akalin et al. 2012a). The ERRBS raw data were aligned to the whole genome, and the methylation was called using the epigenetic core pipeline at Weill Cornell Medical School. The differential methylated CpGs were identified with the methylKit R package (Akalin et al. 2012b). The data were processed and plotted using R script. The two-dimensional (2D) hierarchical clustering of 21 chondrosarcoma samples was performed using the heat map function in R 2.15.1 (<http://www.r-project.org>) with 1-Pearson correlation distance and Ward's agglomeration method. The ERRBS data have been deposited in the NCBI's Gene Expression Omnibus (accession no. GSE50539).

GSEA

Gene sets from the Broad Institute Molecular Signatures Database (<http://www.broadinstitute.org/gsea/msigdb/index.jsp>) were used. The overrepresentation of gene sets in the gene list was done using hypergeometric calculation implemented in the GOstats Bioconductor package (<http://www.bioconductor.org/packages/release/bioc/html/GOstats.html>) in R statistical language (<http://www.r-project.org>). Gene ontology analysis was performed with the online software DAVID on functional analysis of gene lists (Huang et al. 2009).

Plasmid construction

The cDNA clone of human IDH2 (BC009244) was purchased from Invitrogen in pOTB7. Standard site-directed mutagenesis

techniques were used to make IDH2 R172K by introducing a g515a change in the IDH2 ORF. Wild-type and mutant sequences were then subcloned into the LPC vector, and IDH2 R172K/A174D was made by introducing a c521a change in the ORF of the LPC-IDH2 R172K construct. All sequences were confirmed by direct sequencing before retrovirus generation.

Cell culture, transfection/transduction, and generation of stable cell lines

C3H10T1/2 cells were cultured in Dulbecco's modified Eagle's medium (DMEM; Invitrogen) with 10% fetal bovine serum (FBS; CellGro). To generate 10T cell lines with stable expression of wild-type or mutant IDH2, supernatant from 293T cells transfected with pCL-Eco helper virus and plasmids was collected after 72 h, filtered, and applied to 10T parental cells overnight. Pooled populations of puromycin-resistant cells were obtained by growing cells in 2.5 µg/mL puromycin for 7 d following retroviral transduction and then continuously culturing in puromycin.

10T cell differentiation

Adipocyte differentiation of 10T cells was done following the same procedure as 3T3-L1 cell differentiation previously described (Wellen et al. 2009). In brief, confluent 10T cells were stimulated with a cocktail containing 0.5 mM isobutylmethylxanthine, 1 µM dexamethasone, 5 µg/mL insulin, and 5 µM troglitazone (all from Sigma) in DMEM with 10% FBS to induce differentiation. Cells were maintained in DMEM with insulin after 2 d of differentiation until they were ready to be harvested. Chondrocyte differentiation of 10T cells was performed as previously described (Mikami et al. 2011). In brief, confluent 10T cells were stimulated with a cocktail containing DMEM with 1% FBS, 10 µg/mL human insulin (Sigma), 3×10^{-8} M sodium selenite (Sigma), 10 µg/mL human transferrin (Sigma), 10^{-8} M dexamethasone, and 100 ng/mL rhBMP-2 (R&D Systems). Medium was replaced with fresh cocktail every 2–3 d until cells were ready to be imaged or harvested.

Histone extraction and Western blotting

For histone acid extraction, cells were lysed in hypotonic lysis buffer (10 mM HEPES, 10 mM KCl, 1.5 mM MgCl₂, 0.5 mM DTT, protease inhibitors) for 1 h. H₂SO₄ was added to 0.2 N followed by overnight rotation at 4°C. After centrifugation, supernatants were collected, and proteins were precipitated in 33% TCA, washed with acetone, and resuspended in deionized water. For whole-cell lysates, cells were lysed in standard RIPA buffer (1% NaDOC, 0.1% SDS, 1% Triton X-100, 0.01 M Tris at pH 8.0, 0.14 M NaCl), and lysates were then sonicated and centrifuged at 14,000g at 4°C. Supernatants were collected and normalized for total protein concentration, separated by SDS-PAGE, transferred to nitrocellulose membrane, blocked in 5% nonfat milk in PBS plus 0.5% Tween 20, probed with primary antibodies, and detected with horseradish peroxidase-conjugated anti-rabbit or anti-mouse secondary antibodies (GE Healthcare, NA934V and NA931V). The primary antibodies used include anti-IDH2 (Abcam, ab55271), anti-H3K9me2 (Cell Signaling Technology, 9753), anti-H3K9me3 (Active Motif, 39765), anti-H3K36me3 (Abcam, ab9050), anti-H3K27me3 (Millipore, 07-449), anti-H3K4me3 (Active Motif, 39916), anti-H3K79me2 (Cell Signaling Technology, 9757), anti-acetyl H3 (Upstate Biotechnology, 06-599), anti-H3 (Cell Signaling Technology, 4499), anti-tubulin (Sigma, T9026), anti-cyclin D1 (EMD Millipore, CC12), anti-p27 (Santa Cruz Biotechnology, sc-1641), anti-N-cadherin (Cell Signaling Tech, 4061).

Metabolite extraction and gas chromatography (GC)-MS analysis

Frozen chondrosarcoma tissue (30–60 mg) or 10T cells were homogenized in 1.2 mL of ice-cold 80% methanol containing 20 μ M deuterated 2HG as an internal standard (D-hydroxyglutaric-2,3,3,4,4- d_5) using a tissue homogenizer (Omni International). Methanol extracts were incubated for 30 min at -80°C and centrifuged at 21,000g for 20 min at 4°C to remove precipitated protein. Five-hundred microliters of extracts was evaporated to dryness under a nitrogen gas stream. Dried organic acids were derivatized by the addition of 20 μ L of 40 mg/mL methoxyamine hydrochloride in pyridine with incubation for 90 min at 30°C followed by 80 μ L of MSTFA + 1% TMCS (Thermo Scientific) with incubation for 30 min at 37°C . One microliter of the trimethylsilyl-derivatized organic acids was analyzed by GC-MS using an Agilent 7890A GC equipped with an HP-5MS capillary column and connected to an Agilent 5975 C mass selective detector operating in splitless mode with electron impact ionization. Relative quantification of 2HG was determined from extracted ion chromatograms for 2HG (m/z : 349) normalized to either the d_5 -2HG internal standard (m/z : 354) or citrate (m/z : 465) and corrected by wet weight of tissue sample or cell numbers.

Cell proliferation and cell cycle analysis

EdU incorporation assay was performed using the Click-iT EdU flow cytometry assay kit (Invitrogen, C10425) according to the manufacturer's instructions. In brief, 10T cells at sparse or post-confluence were incubated with 10 μ M EdU for 4 h. Cells were then trypsinized, washed with PBS, and fixed for 15 min at room temperature. After fixation, cells were washed with PBS and incubated in permeabilization buffer containing CuSO_4 and Alexa Fluor 448 azide for 30 min at room temperature. Levels of EdU incorporation were measured using a Becton Dickinson Calibur flow cytometer.

For FACS analysis of cell cycle distribution, adherent cells in a six-well plate were trypsinized and collected in 15-mL centrifuge tubes. The collected cells were fixed by ethanol (final concentration of 70%) overnight at -20°C . Cells were then stained with 50 μ g/mL propidium iodide (Sigma) with 0.1 mg/mL RNase A for 40 min at 37°C . After washing with PBS, the DNA content of the stained cells was then analyzed by a Becton Dickinson Calibur flow cytometer.

Quantitative real-time PCR

RNA was isolated using TRIzol (Invitrogen). After incubating with DNase, cDNA was synthesized using SuperScript II reverse transcriptase (Invitrogen). Quantitative PCR was performed on a 7900HT sequence detection system (Applied Biosystems) using TaqMan gene expression assays (Applied Biosystems). Gene expression data were normalized to 18S rRNA.

Immunohistochemical staining

Immunohistochemical detection was performed using the Discovery XT processor (Ventana Medical Systems). Paraffin-embedded tissue sections were blocked for 30 min in 10% normal goat serum plus 2% BSA in PBS. Sections were incubated for 5 h with 0.4 μ g/mL rabbit polyclonal anti-Ki67 (Vector Laboratories, VP-K451), 1 μ g/mL mouse monoclonal anti-p27 (BD Biosciences, 55890), or 6 μ g/mL rabbit polyclonal anti-Cyclin D1 (Santa Cruz Biotechnology, H-295) antibodies. Tissue sections were then incubated for 60 min with biotinylated goat anti-rabbit IgG

(Vector Laboratories, PK6101) or goat anti-mouse IgG (Vector Laboratories, BA9200) at 1:200 dilutions. Blocker D, streptavidin-HRP, and the DAB detection kit (Ventana Medical Systems) were used according to the manufacturer's instructions.

Tumor xenograft study

10T cells were harvested with trypsin and resuspended in PBS. Approximately 10^7 cells were injected subcutaneously into both flanks of 6- to 8-wk-old athymic female nude mice (Harlan Laboratories). Formation of tumors was monitored. After tumors became palpable, tumor volumes were estimated by caliper measurements, assuming spherical geometry (volume = $d^3 \times \pi/6$). Mice were cared for in accordance with the institutional animal care and use committee at Memorial Sloan-Kettering Cancer Center.

Structural modeling

The active site of human IDH2 with isocitrate was modeled based on the highly homologous porcine IDH2 crystal structure, as previously described (Ward et al. 2010, 2012).

Dot blot

Genomic DNA was phenol-chloroform-extracted and quantified using NanoDrop. DNA was denatured with 0.1 M NaOH, serially diluted, and spotted on a nitrocellulose membrane. 5mC antibody (Millipore, MABE146) was used at 1:2000 dilution.

Statistical analysis

Statistical analysis was performed using a Student's *t*-test (two-sample equal variance; two-tailed distribution) unless stated otherwise.

Acknowledgments

We thank members of the Thompson laboratory for technical help and critical reading of the manuscript. We thank the Memorial Sloan-Kettering Cancer Center (MSKCC) Molecular Cytology Core Facility for technical help with the immunohistochemical study, the MSKCC Anti-tumor Assessment Core Facility for technical help with the mouse xenograft study, and the Epigenomics Core Facility of Weill Cornell Medical College for help with ERRBS. This work was supported by the Starr Cancer Consortium, grants from NCI and NIH (to C.B.T.), a Specialized Center of Research (SCOR) grant from the Leukemia and Lymphoma Society (to S.W.L.), and a U01 CTDD award from the National Cancer Institute (to S.W.L.). S.W.L. is the Geoffrey Beene Chair of Cancer Biology at MSKCC and an Investigator in the Howard Hughes Medical Institute. C.C. receives a career development fellowship from the Leukemia and Lymphoma Society. P.S.W. was supported in part by the University of Pennsylvania Medical Scientist Training Program. J.H.H. is funded by the Stephen McDermott Chair in Surgery.

References

- Akalin A, Garrett-Bakelman FE, Kormaksson M, Busuttill J, Zhang L, Khrebukova I, Milne TA, Huang Y, Biswas D, Hess JL, et al. 2012a. Base-pair resolution DNA methylation sequencing reveals profoundly divergent epigenetic landscapes in acute myeloid leukemia. *PLoS Genet* 8: e1002781.
- Akalin A, Kormaksson M, Li S, Garrett-Bakelman FE, Figueroa ME, Melnick A, Mason CE. 2012b. methylKit: A compre-

- hensive R package for the analysis of genome-wide DNA methylation profiles. *Genome Biol* **13**: R87.
- Amary MF, Bacsi K, Maggiani F, Damato S, Halai D, Berisha F, Pollock R, O'Donnell P, Grigoriadis A, Diss T, et al. 2011a. IDH1 and IDH2 mutations are frequent events in central chondrosarcoma and central and periosteal chondromas but not in other mesenchymal tumours. *J Pathol* **224**: 334–343.
- Amary MF, Damato S, Halai D, Eskandarpour M, Berisha F, Bonar F, McCarthy S, Fantin VR, Straley KS, Lobo S, et al. 2011b. Ollier disease and Maffucci syndrome are caused by somatic mosaic mutations of IDH1 and IDH2. *Nat Genet* **43**: 1262–1265.
- Arai M, Nobusawa S, Ikota H, Takemura S, Nakazato Y. 2012. Frequent IDH1/2 mutations in intracranial chondrosarcoma: A possible diagnostic clue for its differentiation from chordoma. *Brain Tumor Pathol* **29**: 201–206.
- Bracken AP, Dietrich N, Pasini D, Hansen KH, Helin K. 2006. Genome-wide mapping of Polycomb target genes unravels their roles in cell fate transitions. *Genes Dev* **20**: 1123–1136.
- Chowdhury R, Yeoh KK, Tian YM, Hillringhaus L, Bagg EA, Rose NR, Leung IK, Li XS, Woon EC, Yang M, et al. 2011. The oncometabolite 2-hydroxyglutarate inhibits histone lysine demethylases. *EMBO Rep* **12**: 463–469.
- Dang L, White DW, Gross S, Bennett BD, Bittinger MA, Driggers EM, Fantin VR, Jang HG, Jin S, Keenan MC, et al. 2009. Cancer-associated IDH1 mutations produce 2-hydroxyglutarate. *Nature* **462**: 739–744.
- Figuerola ME, Abdel-Wahab O, Lu C, Ward PS, Patel J, Shih A, Li Y, Bhagwat N, Vasanthakumar A, Fernandez HF, et al. 2010. Leukemic IDH1 and IDH2 mutations result in a hypermethylation phenotype, disrupt TET2 function, and impair hematopoietic differentiation. *Cancer Cell* **18**: 553–567.
- Gumbiner BM. 2005. Regulation of cadherin-mediated adhesion in morphogenesis. *Nat Rev Mol Cell Biol* **6**: 622–634.
- Huang DW, Sherman BT, Lempicki RA. 2009. Systematic and integrative analysis of large gene lists using DAVID bioinformatics resources. *Nat Protoc* **4**: 44–57.
- Li S, Chou AP, Chen W, Chen R, Deng Y, Phillips HS, Selfridge J, Zurayk M, Lou JJ, Everson RG, et al. 2013. Overexpression of isocitrate dehydrogenase mutant proteins renders glioma cells more sensitive to radiation. *Neuro Oncol* **15**: 57–68.
- Losman JA, Looper RE, Koivunen P, Lee S, Schneider RK, McMahon C, Cowley GS, Root DE, Ebert BL, Kaelin WG Jr. 2013. (R)-2-hydroxyglutarate is sufficient to promote leukemogenesis and its effects are reversible. *Science* **339**: 1621–1625.
- Lu C, Ward PS, Kapoor GS, Rohle D, Turcan S, Abdel-Wahab O, Edwards CR, Khanin R, Figuerola ME, Melnick A, et al. 2012. IDH mutation impairs histone demethylation and results in a block to cell differentiation. *Nature* **483**: 474–478.
- Mardis ER, Ding L, Dooling DJ, Larson DE, McLellan MD, Chen K, Koboldt DC, Fulton RS, Delehaunty KD, McGrath SD, et al. 2009. Recurring mutations found by sequencing an acute myeloid leukemia genome. *N Engl J Med* **361**: 1058–1066.
- Mikami Y, Ishii Y, Watanabe N, Shirakawa T, Suzuki S, Irie S, Isokawa K, Honda MJ. 2011. CD271/p75(NTR) inhibits the differentiation of mesenchymal stem cells into osteogenic, adipogenic, chondrogenic, and myogenic lineages. *Stem Cells Dev* **20**: 901–913.
- Mullarky E, Mattaini KR, Vander Heiden MG, Cantley LC, Locasale JW. 2011. PHGDH amplification and altered glucose metabolism in human melanoma. *Pigment Cell Melanoma Res* **24**: 1112–1115.
- Noushmehr H, Weisenberger DJ, Diefes K, Phillips HS, Pujara K, Berman BP, Pan F, Pelloski CE, Sulman EP, Bhat KP, et al. 2010. Identification of a CpG island methylator phenotype that defines a distinct subgroup of glioma. *Cancer Cell* **17**: 510–522.
- Oermann EK, Wu J, Guan KL, Xiong Y. 2012. Alterations of metabolic genes and metabolites in cancer. *Semin Cell Dev Biol* **23**: 370–380.
- Pansuriya TC, van Eijk R, d'Adamo P, van Ruler MA, Kuijjer ML, Oosting J, Cleton-Jansen AM, van Oosterwijk JG, Verbeke SL, Meijer D, et al. 2011. Somatic mosaic IDH1 and IDH2 mutations are associated with enchondroma and spindle cell hemangioma in Ollier disease and Maffucci syndrome. *Nat Genet* **43**: 1256–1261.
- Reznikoff CA, Brankow DW, Heidelberger C. 1973. Establishment and characterization of a cloned line of C3H mouse embryo cells sensitive to postconfluence inhibition of division. *Cancer Res* **33**: 3231–3238.
- Rohle D, Popovici-Muller J, Palaskas N, Turcan S, Grommes C, Campos C, Tsoi J, Clark O, Oldrini B, Komisopoulou E, et al. 2013. An inhibitor of mutant IDH1 delays growth and promotes differentiation of glioma cells. *Science* **340**: 626–630.
- Sasaki M, Knobbe CB, Itsumi M, Elia AJ, Harris IS, Chio II, Cairns RA, McCracken S, Wakeham A, Haight J, et al. 2012a. D-2-hydroxyglutarate produced by mutant IDH1 perturbs collagen maturation and basement membrane function. *Genes Dev* **26**: 2038–2049.
- Sasaki M, Knobbe CB, Munger JC, Lind EF, Brenner D, Brustle A, Harris IS, Holmes R, Wakeham A, Haight J, et al. 2012b. IDH1(R132H) mutation increases murine haematopoietic progenitors and alters epigenetics. *Nature* **488**: 656–659.
- Schechtman LM. 2012. Rodent cell transformation assays—a brief historical perspective. *Mutat Res* **744**: 3–7.
- Squazzo SL, O'Geen H, Komashko VM, Krig SR, Jin VX, Jang SW, Margueron R, Reinberg D, Green R, Farnham PJ. 2006. Suz12 binds to silenced regions of the genome in a cell-type-specific manner. *Genome Res* **16**: 890–900.
- Taylor SM, Jones PA. 1979. Multiple new phenotypes induced in 10T1/2 and 3T3 cells treated with 5-azacytidine. *Cell* **17**: 771–779.
- Tsai HC, Li H, Van Neste L, Cai Y, Robert C, Rassool FV, Shin JJ, Harbom KM, Beaty R, Pappou E, et al. 2012. Transient low doses of DNA-demethylating agents exert durable antitumor effects on hematological and epithelial tumor cells. *Cancer Cell* **21**: 430–446.
- Turcan S, Rohle D, Goenka A, Walsh LA, Fang F, Yilmaz E, Campos C, Fabius AW, Lu C, Ward PS, et al. 2012. IDH1 mutation is sufficient to establish the glioma hypermethylator phenotype. *Nature* **483**: 479–483.
- Vander Heiden MG, Cantley LC, Thompson CB. 2009. Understanding the Warburg effect: The metabolic requirements of cell proliferation. *Science* **324**: 1029–1033.
- Wang F, Travins J, Delabarre B, Penard-Lacronique V, Schalm S, Hansen E, Straley K, Kernytsky A, Liu W, Gliser C, et al. 2013. Targeted inhibition of mutant IDH2 in leukemia cells induces cellular differentiation. *Science* **340**: 622–626.
- Warburg O. 1956. On the origin of cancer cells. *Science* **123**: 309–314.
- Ward PS, Thompson CB. 2012. Metabolic reprogramming: A cancer hallmark even Warburg did not anticipate. *Cancer Cell* **21**: 297–308.
- Ward PS, Patel J, Wise DR, Abdel-Wahab O, Bennett BD, Collier HA, Cross JR, Fantin VR, Hedvat CV, Perl AE, et al. 2010. The common feature of leukemia-associated IDH1 and IDH2 mutations is a neomorphic enzyme activity converting α -ketoglutarate to 2-hydroxyglutarate. *Cancer Cell* **17**: 225–234.

- Ward PS, Cross JR, Lu C, Weigert O, Abel-Wahab O, Levine RL, Weinstock DM, Sharp KA, Thompson CB. 2012. Identification of additional IDH mutations associated with oncometabolite R(-)-2-hydroxyglutarate production. *Oncogene* **31**: 2491–2498.
- Ward PS, Lu C, Cross JR, Abdel-Wahab O, Levine RL, Schwartz GK, Thompson CB. 2013. The potential for isocitrate dehydrogenase mutations to produce 2-hydroxyglutarate depends on allele specificity and subcellular compartmentalization. *J Biol Chem* **288**: 3804–3815.
- Wellen KE, Hatzivassiliou G, Sachdeva UM, Bui TV, Cross JR, Thompson CB. 2009. ATP-citrate lyase links cellular metabolism to histone acetylation. *Science* **324**: 1076–1080.
- Williams K, Christensen J, Helin K. 2012. DNA methylation: TET proteins—guardians of CpG islands? *EMBO Rep* **13**: 28–35.
- Wu H, Zhang Y. 2011. Tet1 and 5-hydroxymethylation: A genome-wide view in mouse embryonic stem cells. *Cell Cycle* **10**: 2428–2436.
- Xu W, Yang H, Liu Y, Yang Y, Wang P, Kim SH, Ito S, Yang C, Xiao MT, Liu LX, et al. 2011. Oncometabolite 2-hydroxyglutarate is a competitive inhibitor of α -ketoglutarate-dependent dioxygenases. *Cancer Cell* **19**: 17–30.
- Yan H, Parsons DW, Jin G, McLendon R, Rasheed BA, Yuan W, Kos I, Batinic-Haberle I, Jones S, Riggins GJ, et al. 2009. IDH1 and IDH2 mutations in gliomas. *N Engl J Med* **360**: 765–773.